Materiales de Construcción
Vol. 74, Issue 354, April-June 2024, e343
ISSN-L: 0465-2746
https://doi.org/10.3989/mc.2024.359623

Transport properties of fly ash-slag-based geopolymer concrete with 2M sodium hydroxide combined with variations in slag percentage, Al/Bi ratio, and SS/SH ratio

E.S. Sunarsih[a] ✉, S. As'ad[a], A.R. Mohd Sam[b], S.A. Kristiawan[a]

a. Department of Civil Engineering, Faculty of Engineering, Sebelas Maret University, (Surakarta, Indonesia)
b. UTM Construction Research Centre, Institute for Smart Infrastructure and Innovative Construction, Faculty of Civil Engineering, Universiti Teknologi Malaysia, (Johor, Malaysia)
✉: ernawatisri@staff.uns.ac.id

Received 10 July 2023
Accepted 29 November 2023
Available on line 23 May 2024

ABSTRACT: The aim of this research is to determine the effect of sodium hydroxide molarity 2M combined with variations in slag percentage, ratio of alkali activator to binder (Al/Bi), and ratio of sodium silicate to sodium hydroxide (SS/SH) on the transport properties of fly ash-slag-based GPC cured at ambient temperature. The result is increase in slag percentage and SS/SH ratio lead to a decrease in porosity, water absorption rate and chloride permeability. The alkali activator to binder (Al/Bi) ratio of 0.45 produces the lowest porosity, water absorption rate, and chloride permeability. The porosity, sorptivity, and chloride penetration depths of all GPC are lower than those of OPC. The recommended mix compositions for GPC that exhibit lower transport properties than OPC are GPC4 (slag 40%, SS/SH ratio 1.5, Al/Bi ratio 0.45); GPC5 (slag 50%, SS/SH ratio 1.5, Al/Bi ratio 0.45); and GPC7 (slag 30%, SS/SH ratio 2.0, Al/Bi ratio 0.45).

KEY WORDS: Molarity sodium hydroxide; Porosity; Sorptivity; Chloride permeability; Fly ash-slag-based geopolymer.

Citation/Citar como: Sunarsih ES, As'ad S, Mohd Sam AR, Kristiawan SA. 2024. Transport properties of fly ash-slag-based geopolymer concrete with 2M sodium hydroxide combined with variations in slag percentage, Al/Bi ratio, and SS/SH ratio. Mater. Construcc. 74(354):e343. https://doi.org/10.3989/mc.2024.359623.

RESUMEN: *Propiedades de transporte del hormigón geopolímero fabricado con escorias y cenizas volantes con hidróxido de sodio 2M con variaciones en el porcentaje de escoria, la relación Al/Bi y la relación SS/SH.* El objetivo de esta investigación es determinar el efecto de la molaridad de hidróxido de sodio 2M combinado con variaciones en el porcentaje de escoria, la relación de activador alcalino/binder (Al/Bi) y la relación de silicato de sodio/hidróxido de sodio (SS/SH) sobre las propiedades de transporte del GPC a base de escoria y cenizas volantes curado a temperatura ambiente. Los resultados indican que un aumento en el porcentaje de escoria y en la relación SS/SH conducen a una disminución de la porosidad, la tasa de absorción de agua y la permeabilidad al cloruro. La proporción de activador alcalino/binder (Al/Bi) de 0,45 produce disminuciones en la porosidad, la tasa de absorción de agua y la permeabilidad al cloruro. La porosidad, la sortividad y las profundidades de penetración de cloruro de todos los GPC son menores que las del OPC. Las composiciones de mezcla recomendadas para GPC que exhiben propiedades de transporte más bajas que el OPC son GPC4 (escoria 40 %, relación SS/SH 1,5, relación Al/Bi 0,45); GPC5 (escoria 50 %, relación SS/SH 1,5, relación Al/Bi 0,45); y GPC7 (escoria 30%, relación SS/SH 2,0, relación Al/Bi 0,45).

PALABRAS CLAVE: Molaridad de hidróxido de sodio; Porosidad; Sortividad; Permeabilidad al cloruro; Geopolímero basado en cenizas volantes y escorias.

1. INTRODUCTION

The production of Portland cement has been found to be a leading contributor to the release of greenhouse gas emissions into the atmosphere, particularly carbon dioxide (CO_2). An estimated 0.95 tons of CO_2 are released for each ton of the cement produced (1). It has been further found that of the total CO_2 emissions associated with concrete production, a staggering 76-80% is attributed to the production of the cement (2, 3). In fact, these CO_2 emissions account for about 75% of all greenhouse gas emissions (4). This alarming rate of emission necessitates the need to develop alternative binders to reduce the environmental impact of cement production.

Geopolymer binder, which releases 80–90% lower CO_2 emissions, currently represents one prospective alternative binder that can considerably minimize the environmental impact (1). Geopolymer binder is created by activating precursors that contain aluminosilicates like fly ash, silica fume, ground granulated blast furnace slag, and metakaolin, with an alkaline activator such as sodium hydroxide (SH), sodium silicate (SS), sodium sulfate or carbonate, potassium hydroxide (KOH) and potassium silicate (K_2SiO_3) (5–7). The matrix and strength of this type of cement does not require the formation of hydrated calcium silicate (C-S-H) gel, as with ordinary Portland cement concrete (OPC), but instead relies on aluminosilicate polycondensation (8). When a low calcium precursor is used to create geopolymer binder, a sodium aluminum silicate hydrate (N-A-S-H) gel with a three-dimensional structure is produced (9).

Many studies have focused on GPC made from low-calcium fly ash and using SS and SH as an alkali activator. However, the moderate temperature curing required for this type of geopolymer limits its practical use (10–13). To address this issue, researchers have explored the potential of new geopolymer formulas that can be cured at lower temperatures. One possible solution is to increase the calcium content in the binder by introducing slag, which has high calcium content, to the low-calcium fly ash-based geopolymer mixture. This can enhance the mechanical and microstructural properties of GPC by promoting the formation of hydrated calcium aluminum silicate (C-A-S-H) gel, the primary product of polymerization (14–17).

Geopolymer concrete with 20% fly ash substitution with slag has higher strength than that made from 100% fly ash. One positive finding is that when cured at room temperature, using 100% slag results in the highest strength (7). The addition of slag also reduces pore size and porosity, ultimately decreasing the amount of water it can absorb over a period of time (18). The reduction could be identified concerning the water absorption rate with time. At first, the water absorption rate in GPC was relatively high because of the absorption of pores at a size larger than 200 nm. Over time, the rate diminishes. In contrast, the water absorption rate in OPC specimens initially starts low due to fewer pores with a size larger than 200 nm but continues to increase. Another report indicated that the water absorption rate of GPC containing 30% slag was comparable to that of OPC specimens (19). Other research showed that by using a higher slag percentage and lower SS/SH ratio in GPC, shrinkage can be decreased, making it comparable to OPC (20). It has been observed that as more fly ash substitution by slag in GPC, the water absorption, sorptivity, and porosity of the material are all reduced (21, 22). This phenomenon is due to the slag and alkaline activator reaction, resulting the formation of denser C-A-S-H gels than the N-A-S-H gels (18). Furthermore, the smaller size of slag particles makes them function as micro fillers (23).

Research has shown that GPC has comparable or even superior physical and mechanical properties to OPC. In terms of durability, GPC has been studied for its resistance to aggressive environments, including sulfate attack, chloride ingress, carbon dioxide penetration, and acids (24). Chloride ingress can destroy the passivation layer on the steel reinforcement, trigger corrosion caused by electrochemistry, and subsequently, decrease the structural strength of concrete. Although chlorides can have such detrimental effect, they generally do not disintegrate the concrete matrix since the rates of degradation caused by chlorides are shown to be lower (25). Many researchers found that compared to GPC, OPC demonstrated a greater capacity to bind chloride. This is because of the reaction among the AFm phase (alumina, iron oxide, mono sulphate) in OPC with chloride ions, forming Friedel salts. On the other hand, GPC has a minimal ability to bind chloride as there is no visible reaction between the geopolymer binder and chloride ions; however, the ability to bind chloride is dependent on the adsorption or encapsulation of chloride in the network of geopolymer pores (25–27).

Through the use of the Rapid Chloride Permeability Test (RCPT), a comparative study was conducted to analyze the chloride permeability of OPC and fly ash-based GPC. The results showed that the permeability of OPC and fly ash-based GPC is similar when compared using the same compressive strength. Nevertheless, the addition of a higher proportion of slag to the geopolymer concrete leads to a decrease in the total charge passed and a change in the permeability classification of the concrete (22, 28). The reduction in concrete permeability is due to the addition of hydrated compounds based on calcium, which act as micro aggregates and coexist with the geopolymeric components to create a dense microstructure that impedes the infiltration of water from the capillary pores. Furthermore, slag is more reactive than fly ash particles in alkaline media, making it easier for the abundantly available alumina and silica ions to dissolve and improve the polycondensation mechanism

(22, 29). The total charge passed decreases with extended curing time, as a denser matrix of geopolymer is created, impeding the penetration of chloride ions (30).

GPC is much more resistant to chloride attack, showing a longer time to experience cracking due to chloride-induced corrosion in comparison to OPC. At 40 mm depth, GPC's chloride content is ten times lesser than that of OPC, which is insufficient to initiate chloride-induced corrosion (31). Additionally, the pore structure of GPC becomes disconnected as it matures (5). With increasing curing time of GPC, the porosity is reduced owing to the space-filling properties of the C-(N)-A-S-H phase (18). The main reaction products of GPC with slag content are C-S-H, C-A-S-H, N-A-S-H, and the hydrotalcite phase, with an increase of slag content resulting in greater amounts of C-S-H and C-A-S-H, as well as an increase in the hydrotalcite phase. C-A-S-H has a higher ability than N-A-S-H to bind chloride ions, reducing their entry (25). Hydrotalcite ($Mg_6Al_2(OH)16CO_34H_2O$) is a compound that has a double-layered hydroxide structure. This layered crystal structure consists of an outer layer with hydroxides and an inner layer with anions and water molecules. The addition of hydrotalcite to externally contaminated chloride-contaminated concrete results in a reduction in the chloride content in the concrete compared to without the hydrotalcite structure (32).

To date, research on fly ash-slag-based GPC has predominantly employed sodium hydroxide solution with moderate to high molarity (16, 22, 33–35), resulting in significant CO_2 emissions during the production of alkaline activator solution (2, 36–38). To address this issue, the present study proposes using a combination of SS and SH molarity of 2M as an alkaline activator to represents a more sustainable GPC that can be cured at room temperature. The use of sodium hydroxide with a molarity of 2M is based on preliminary tests on fly ash-slag-based geopolymer paste and mortar. This test uses variations in SH molarity of 1M, 2M, 4M, 6M, 8M, and 10M, a slag percentage of 30%, the SS/SH ratio of 0.5, 1.0, and 1.5, and the Al/Bi ratio of 0.40, 0.45, and 0.50. Based on the setting time with an SH molarity of 2M, the results were obtained at SS/SH ratios of 1.0 and 1.5, and at all Al/Bi ratios, the final setting time was around 100–160 minutes. Based on the compressive strength of the mortar, the results showed that sodium hydroxide with molarity of 2M had a compressive strength similar to other SH molarities.

Based on these preliminary tests, this research used SH molarity 2M to assess the transport properties of the GPC, focusing on porosity, sorptivity, and chloride permeability properties. The investigation examines the impact of various mixture compositions, such as slag percentages, alkali activator to binder (Al/Bi) ratios, and SS/SH ratios. The results offer insight for engineers seeking to determine the optimal composition of durable and environmentally friendly GPC for practical applications.

2. MATERIALS AND METHODS

2.1. Materials

In this study, the fine aggregate was sourced from Yogyakarta, Indonesia, and coarse aggregate with a nominal diameter of 12.7 mm was obtained from Central Java, Indonesia. The binder materials consisted of type F fly ash from Tanjung Jati B PLTU, Central Java, Indonesia, and slag obtained from PT. Krakatau Semen Indonesia, Banten, Indonesia. Both fly ash and slag must pass sieve no. 200 with a diameter of 75 µm, according to cement fineness specifications (SNI 15-2530-1991). X-ray fluorescence (XRF) testing was employed to determine the chemical compositions of fly ash and slag, and the results are shown in Table 1. The fly ash had a low calcium oxide (about 8.64%) but a high total content of SiO_2, Al_2O_3, and Fe_2O_3 (about 83.8%), so it includes type F fly ash according to ASTM C618 standards. On the other hand, the slag had a high calcium oxide content (about 62.1%).

Alkaline activators were prepared using a mixture of SH and SS, with varying ratios of SS/SH at 1.0, 1.5, and 2.0. The SH solution was created by dissolving 98% pure SH flakes in distilled water, maintaining a constant concentration of 2M across all mixtures. The SS solution used in this study was a commercially available gel with the production code BE-58. Figure 1 and Figure 2 show the raw materials and alkaline activators used in the manufacture the geopolymer concrete.

Table 1. Chemical compositions of fly ash and slag.

Component %	Fly Ash	Slag
SiO_2	41.00	23.50
Al_2O_3	15.00	8.20
Fe_2O_3	26.94	0.95
CaO	8.64	62.10
MgO	0.74	0.30
SO_3	0.50	0.94
K_2O	2.43	0.10
TiO_2	1.71	1.20
Others	2.5	2.61
LoI	0.54	0.1

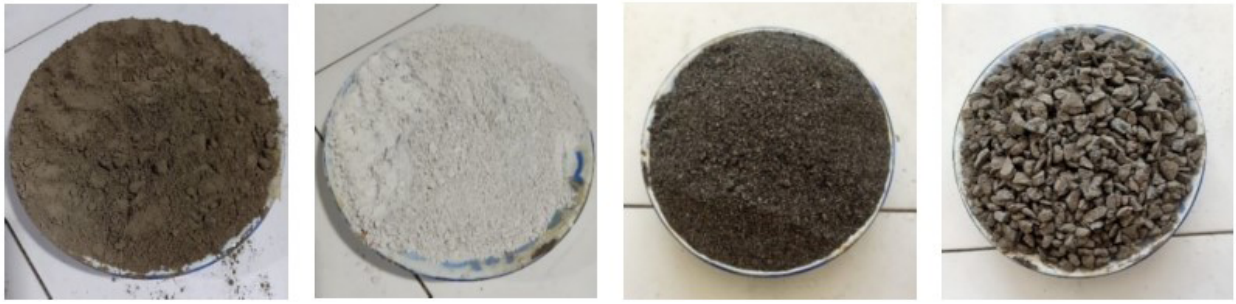

(a) (b) (c) (d)

Figure 1. Materials in GPC (a) Fly ash, (b) Slag, (c) Fine aggregate, and (d) Coarse aggregate.

(a) (b)

Figure 2. Alkaline activators (a) Sodium hydroxide flakes, and (b) Sodium silicate gel.

2.2. Preparation, casting, and curing of specimens

In order to achieve a 25 MPa design strength for normal concrete, the study employed a mixture design that followed the guidelines of SNI 7656:2012 (39), a modified version of ACI 211.1-91 (40) for Indonesian context. The GPC production involved replacing the cement with fly ash and slag, with the slag to total binder percentages ranging from 10% to 50%. To substitute the water-cement ratio, an alkaline activator was utilized with varying Al/Bi ratios of 0.40, 0.45, and 0.50. The aggregates and total binder were kept constant throughout the study. In Table 2, the results of the concrete compressive strength test according to the mix design are presented.

Ten mixtures were produced, consisting of nine GPCs and one OPC as a control (Table 2). The mixtures were designated as GPC1 to GPC9, each with different components. GPC1 to GPC5 were created to investigate the impact of slag percentage. Mixtures GPC3, GPC6, and GPC7 focused on the variations in the SS/SH ratio, while GPC3, GPC8, and GPC9 examined the effects of varying the Al/Bi ratio. The GPC mix designation represented the components of the mixture, for instance, S30-1.5-0.50, indicating a GPC mix with a 30% slag content, the ratio of SS/SH 1.5, and the ratio of Al/Bi 0.50. No additional water or superplasticizer was used in the mixtures.

The GPC mixing process began with the preparation of the necessary materials. A two-molar SH solution was prepared the day before its use, while the alkaline activator, comprising of SS and SH, was mixed and left to settle until it had reached room temperature. After that, a container was filled with a homogeneous mixture of precursor materials, which are fly ash and slag. Then, the GPC constituents were blended in a specific order: sand and coarse aggregate were mixed together for one minute, followed by the addition of a fly ash and slag binder and a two-minute mixing time. The alkaline activator solution was then added according to a precise ratio, and the mixture was given five minutes of blending time to ensure thorough homogeneity.

After the mixing process, the specimens underwent slump testing and were subsequently cast in cylindrical molds with dimensions of 100 mm in diameter and 200 mm in height. The casting was performed in two layers, ensuring compaction in each layer to avoid any cavities. The specimens were allowed to remain in the molds for 24 hours prior to being taken out and cured. For the OPC, curing is done by submerging the specimen in water, while GPC curing involves storing it in an airtight plastic container to maintain moisture at room temperature. Prior to testing, all specimens were shaped into cylindrical forms with a diameter of 100 mm and a height of 50 mm, a process that occurred after 28 days of curing.

Table 2. Mix Proportions.

Mix ID	Designation	Concrete Mixture Quantity (kg/m³)			
		Aggregate (CAg/FAg)	Binder (Fly ash/Slag / Cement)	Activator (SS/SH/Water)	Compressive Strength (MPa)
GPC1	S10-1.5-0.45	858/863	360/40/ -	108/72/ -	23.930
GPC2	S20-1.5-0.45	858/863	320/80/ -	108/72/ -	36.793
GPC3	S30-1.5-0.45	858/863	280/120/ -	108/72/ -	46.667
GPC4	S40-1.5-0.45	858/863	240/160/ -	108/72/ -	50.402
GPC5	S50-1.5-0.45	858/863	200/200/ -	108/72/ -	56.076
GPC6	S30-1.0-0.45	858/863	280/120/ -	90/90/ -	39.620
GPC7	S30-2.0-0.45	858/863	280/120/ -	120/60/ -	38.531
GPC8	S30-1.5-0.40	858/863	280/120/ -	96/64/ -	35.704
GPC9	S30-1.5-0.50	858/863	280/120/ -	120/80/ -	42.839
OPC	-	858/863	- / - /400	- / - /216	27.068

Abbreviations:
CAg: Coarse Aggregate; FAg: Fine aggregate; SS: Sodium Silicate; SH: Sodium Hydroxide

2.3. Testing procedure

2.3.1. Porosity test

The porosity test is specified in ASTM C642-97 (41). The specimen has a cylindrical shape with a height of 50 mm and a 100 mm diameter. The Equation [1] is used to calculate the porosity.

$$Volume\ of\ Permeable\ voids(Porosity)\ (\%) = \frac{(C-A)}{(C-D)} x\ 100 \quad [1]$$

where:
A = Oven-dried specimen mass (g). The test is carried out by drying the sample in an oven at a temperature of 100-110C for no less than 24 hours. Then it is removed from the oven and allowed to cool to a temperature of 20-25C and then the mass is determined.
C = Surface-dry specimen mass in air (g). After immersion and boiling for 5h, let it cool to a temperature of 20-25C. Then remove surface moisture with a dry towel and determine the mass.
D = Apparent mass of specimen in water (g). After the sample has been soaked, boiled and cooled, the next step is to determine the mass of the sample in the water.

2.3.2. Sorptivity test

The sorptivity test, following the procedure outlined in ASTM C1585-13, is conducted to measure the rate of water absorption and sorptivity of a cylindrical specimen. This test involves monitoring the weight change of the specimen as it absorbs water over time (42). The specimens used in this test have a diameter of 100 mm and a height of 50 mm.

To perform the test, the specimen is positioned on supports within a pan filled with tap water. The water level is adjusted to be 1-3 mm above the bottom edge of the specimen, as depicted in Figure 3. The weight of the specimen is then recorded at regular intervals for up to 9 days, following the guidelines of ASTM C1585. These measurements are used to determine the amount of water absorbed, and subsequently calculate the sorptivity value and the rate of water absorption using Equation [2].

$$I = \frac{m_t}{a*d} \quad [2]$$

where:
I = the absorption,
m_t = the increase in specimen weight (g), at time t,
a = the area of exposed surfaces (mm^2)
d = the water density (g/mm^3)

Initial sorptivity ($mm/s^{1/2}$) is identified as the slope of the line acquired from plotting water absorption, ***I,*** to the square root of time ($s^{1/2}$). This slope is determined by utilizing least squares from linear regression, using all of the data from 1 minute to 6 hours. The secondary sorptivity ($mm/s^{1/2}$) is identified as the

slope of the line obtained from plotting water absorption, ***I,*** to the square root of time ($s^{1/2}$) utilizing all the points from 1 to 7 days. The slope was determined using least-square linear regression.

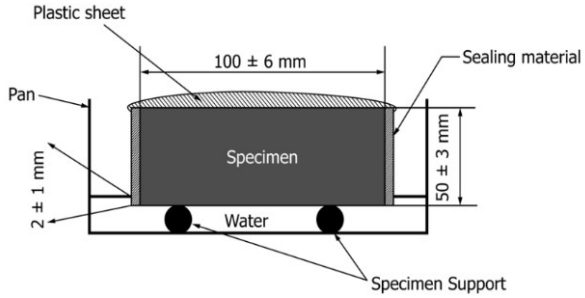

Figure 3. Schematic of the sorptivity test (42).

2.3.3. Rapid Chloride Permeability Test (RCPT)

The Rapid Chloride Permeability Test, as specified by ASTM C1202-12, is used to measure the electrical current passing through cylindrical specimens with a diameter of 100 mm and a height of 50 mm. The test duration is six hours. In this test, a direct current (DC) voltage of 60V is applied to the ends of the specimen. One side of the specimen is submerged in a sodium hydroxide (NaOH) solution, while the other side is submerged in a sodium chloride (NaCl) solution. The overall charge passed through the specimen in Coulombs is then calculated to determine the resistance of the specimen to the penetration of chloride ions (43). As an additional measure, a solution of silver nitrate ($AgNO_3$) is sprayed onto the exposed surface of the concrete to assess the penetration depth of chloride ions. Figure 4 illustrates the configuration of the RCPT test.

Figure 4. Rapid chloride permeability test setup.

3. RESULTS AND DISCUSSION

This research aims to examine how various independent variables, such as different levels of slag in place of fly ash, variations in Al/Bi ratios, and variations in SS/SH ratios at a constant SH molarity of 2M, influence the transport properties of geopolymer concrete (GPC). The results and discussion will be presented separately, based on the type of tests carried out, including porosity, sorptivity, and chloride permeability.

3.1. Porosity

The influence of various independent variables on porosity are presented in Figure 5. Based on Figure 5(a), an increased in the slag content causes the porosity to decrease. The highest reduction value of 10.4% occurs at a slag percentage of 10% and the lowest (7.5%) occurs at 50% slag. The porosity value in OPC is 14.4%. Compared with the OPC, the GPC with slag recorded lower porosity.

The decrease in porosity with increased slag content is likely due to the binder reactions. The formation of C-A-S-H gel is due to the presence of slag, which is denser than geopolymer type gels, resulting in a less porous structure (14, 21). The slag used in this study contains a significantly higher CaO content than fly ash, at 62.1% and 8.6%, respectively (see Table 1). By increasing the amount of slag used in place of fly ash, more C-A-S-H gel will form, which will, in turn, decrease the number of pores in the concrete. In addition, at similar SS/SH ratio, GPC based on fly ash-slag has a larger amount (79%) of 10nm or smaller pores than GPC based on fly ash (16%). This can be attributed to the formation of C-S-H through slag activation in geopolymer concrete, which can fill most of the capillary pores (14). On the other hand, the increased porosity of the fly ash-based GPC is probably related to the gel's binding, mainly in the form of N-A-S-H, which is less dense and more porous (13, 44).

The findings presented in Figure 5(b) suggest that the Al/Bi ratio plays an integral role in porosity. When the ratio reaches 0.45, the minimum porosity of 8.82% is achieved. This can be attributed to the OH^- ions from the alkaline activator, which act as catalysts in the geopolymerization process and facilitate the release of Si^{4+} and Al^{3+} ions from the binder. If the amount of alkaline activator used is less, the leaching process of the aluminum silicate will also be slower, resulting in a poor geopolymeric structure with larger pores and lower strength (28). Meanwhile, at a higher Al/Bi ratio, the amount of alkaline activator used also increases so that the mixture is more dilute. The excess alkaline activator not utilized in the geopolymerization process will eventually become a pore in the concrete after it has hardened. The increasing number of pores causes the porosity to increase and, when compared with OPC, all GPC samples with various Al/Bi ratios have lower porosity.

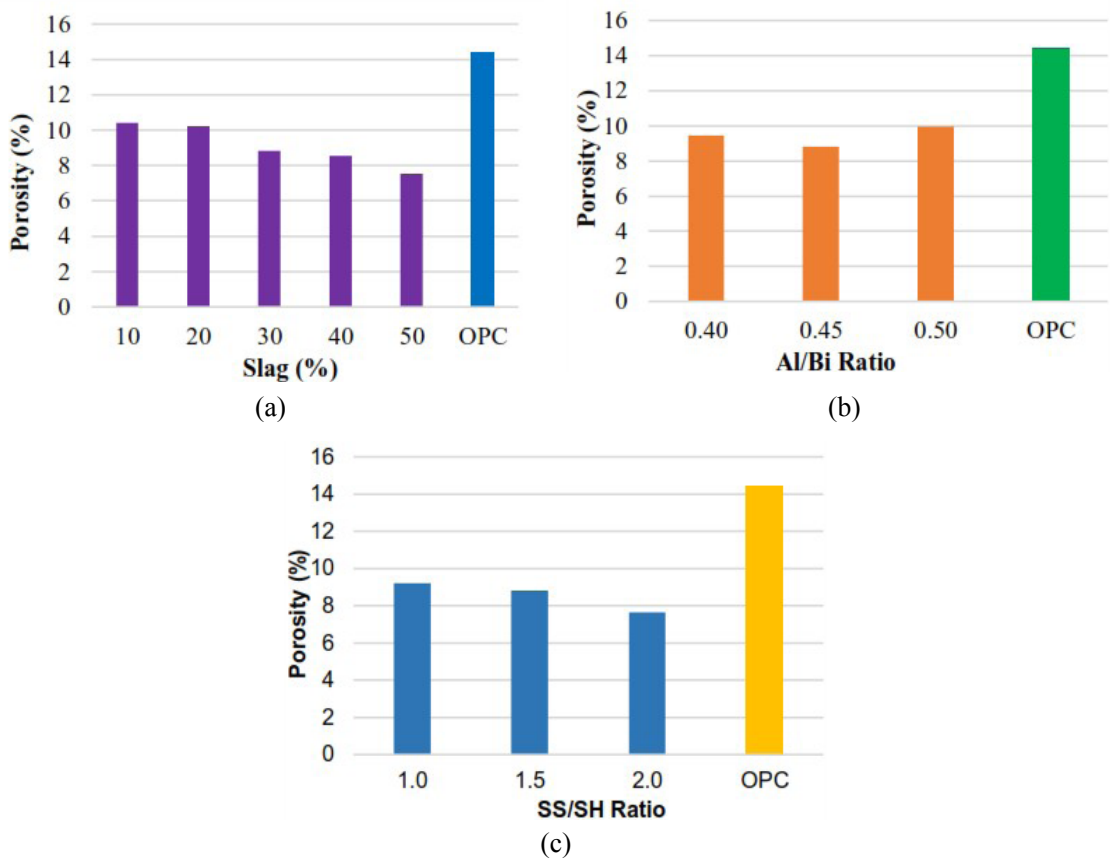

Figure 5. The relationship between (a) porosity and the percentage of slag (SS/SH ratio 1.5, Al/Bi ratio 0.45); (b) porosity and Al/Bi ratio (Slag 30%, SS/SH ratio 1.5); and (c) porosity and SS/SH ratio (slag 30%, Al/Bi ratio 0.45).

Figure 5(c) depicts an increased SS/SH ratio that reduces porosity. The highest porosity of 9.2% was observed for the SS/SH ratio of 1.0. On the other hand, porosity decreased to 8.8% and 7.6% for the SS/SH ratios of 1.5 and 2.0, respectively. The decrease in porosity is due to the higher SS/SH ratio and the higher proportion of sodium silicate results in a greater provision of free silicate. Increasing the amount of silicate in the mixture can increase the polymerization reaction and will form a N-A-S-H gel. Besides that, the presence of high calcium content in the slag will form a denser C-(A)-S-H gel. This is in line with the finding by other researcher (45), who stated that the smaller pores at high SS/SH ratios were due to the increased silica content resulted in a denser polymerized gel with excellent mechanical properties.

According to the description above, porosity is closely related to the number of pores in the concrete. GPC with low molarity SH (2M) and varying slag percentages, Al/Bi ratios, and SS/SH ratios show lower porosity than OPC. This indicates that GPC has fewer pores and a denser structure, which will increase the mechanical properties of concrete.

3.2. Sorptivity

The sorptivity test results indicate that the water absorption rate on the concrete surface and the initial and secondary sorptivity have a strong relationship with the time$^{1/2}$. This can be seen from the data presented in Figure 6, which demonstrates the correlative relationship between the two variables.

The rate of water absorption can be seen in two different phases. Initially, a faster rate of absorption process take place and started to decrease after 1 day. This condition is most likely caused by the pores in the concrete, which are partially saturated (46). In Figure 6(a), the initial absorption of OPC is higher than the other GPC mixtures. However, after 1 day it showed that GPC with 10% slag content (GPC1) had higher absorption than OPC. Based on the data presented in Figure 6(b) and 6(c), it can be observed that all GPC, regardless of the Al/Bi ratios and SS/SH ratios, exhibit lower water absorption values compared to OPC. This trend is observed both at the initial stage of water absorption and throughout the extended water absorption period. This shows that the proportion of the GPC2-GPC9 mixture has resulted smaller pores than OPC.

In accordance with ASTM C1858, the slopes of the graphs in Figure 6 may be used to determine the initial and secondary sorptivity values. However, some requirements must be met, where the graph of the relationship of water absorption with time must show a linear relationship, with a coefficient of correlation of more than 0.98. The sorptivity values obtained through the analysis of these slopes are shown in Figure 7.

Figure 7(a) confirms that a higher percentage of slag used will result in lower initial and secondary sorptivity. Samples with 20%, 30%, 40%, and 50% have initial sorptivities of 10.4, 9.6, 8.2, and 6.0 x 10^{-3} mm/$s^{1/2}$, respectively. The proportion of GPC1 mixture with 10% slag has a slightly different sorptivity value, which has an initial sorptivity of 9 x 10^{-3} mm/$s^{1/2}$, lower than the initial sorptivity of GPC2 and GPC3. However, GPC1 has a greater secondary sorptivity compared to other GPC mixtures. The secondary sorptivity of GPC is much lower than OPC with a very significant difference, except for GPC1. Because GPC1 has the lowest slag content, relatively less C-A-S-H gel is formed, which causes the concrete to be less dense. As a result, GPC1 has the highest secondary sorptivity when compared to other geopolymer concretes. The secondary sorptivity of GPC2, GPC3 and GPC4 is 3.0, 2.0, and 0.8 x 10^{-4} mm/$s^{1/2}$, respectively. Meanwhile, GPC1 has a secondary sorptivity of 12 x 10^{-4} mm/$s^{1/2}$, almost the same as the secondary sorptivity of OPC of 13 x 10^{-4} mm/$s^{1/2}$. Unfortunately, the coefficient of correlation of the GPC5 graph is less than 0.98, so it isn't possible to figure out its secondary sorptivity.

The decline in sorptivity value as the slag content increases signifies that the inclusion of slag in the fly ash-based GPC mixture enhances the microstructural performance, which, in turn, makes the concrete last longer, in terms of water access so that the sorptivity value becomes low (28). The increase of slag will cause the formation of denser C-A-S-H gel with finer pore sizes, thereby preventing water from entering deeper into the concrete (18). In general, the presence of C-A-S-H and N-A-S-H gels in fly ash/slag concrete describes the beneficial behavior that occurs in this material. The formation of N-A-S-H gel during the geopolymerization process is instrumental in reducing the porosity of concrete. This gel fills the voids in the paste and interfaces between the paste and the aggregate, leading to a denser material. The C-A-S-H gel is associated with greater densification and compactness, due to

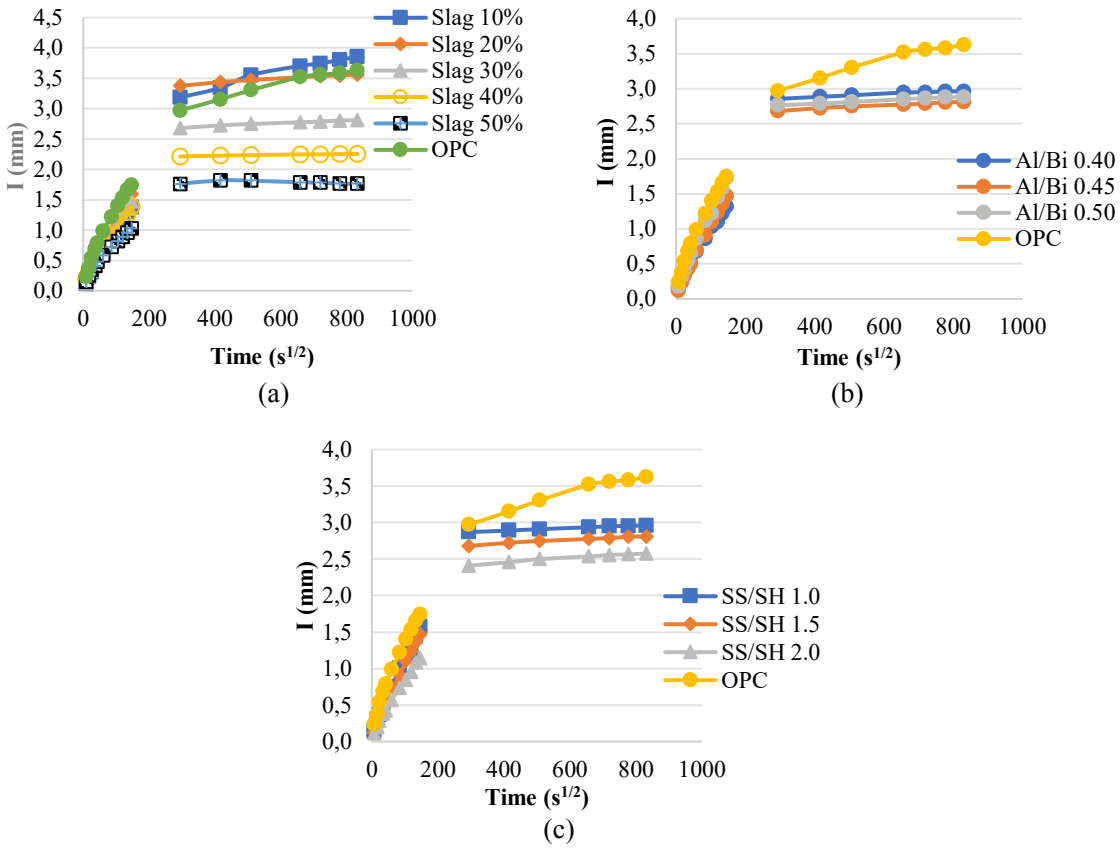

Figure 6. The relationship between time and rate of water absorption on variations in (a) slag percentage (SS/SH ratio 1.5, Al/Bi ratio 0.45); (b) Al/Bi ratio (Slag 30%, SS/SH ratio 1.5); and (c) SS/SH ratio (slag 30%, Al/Bi ratio 0.45).

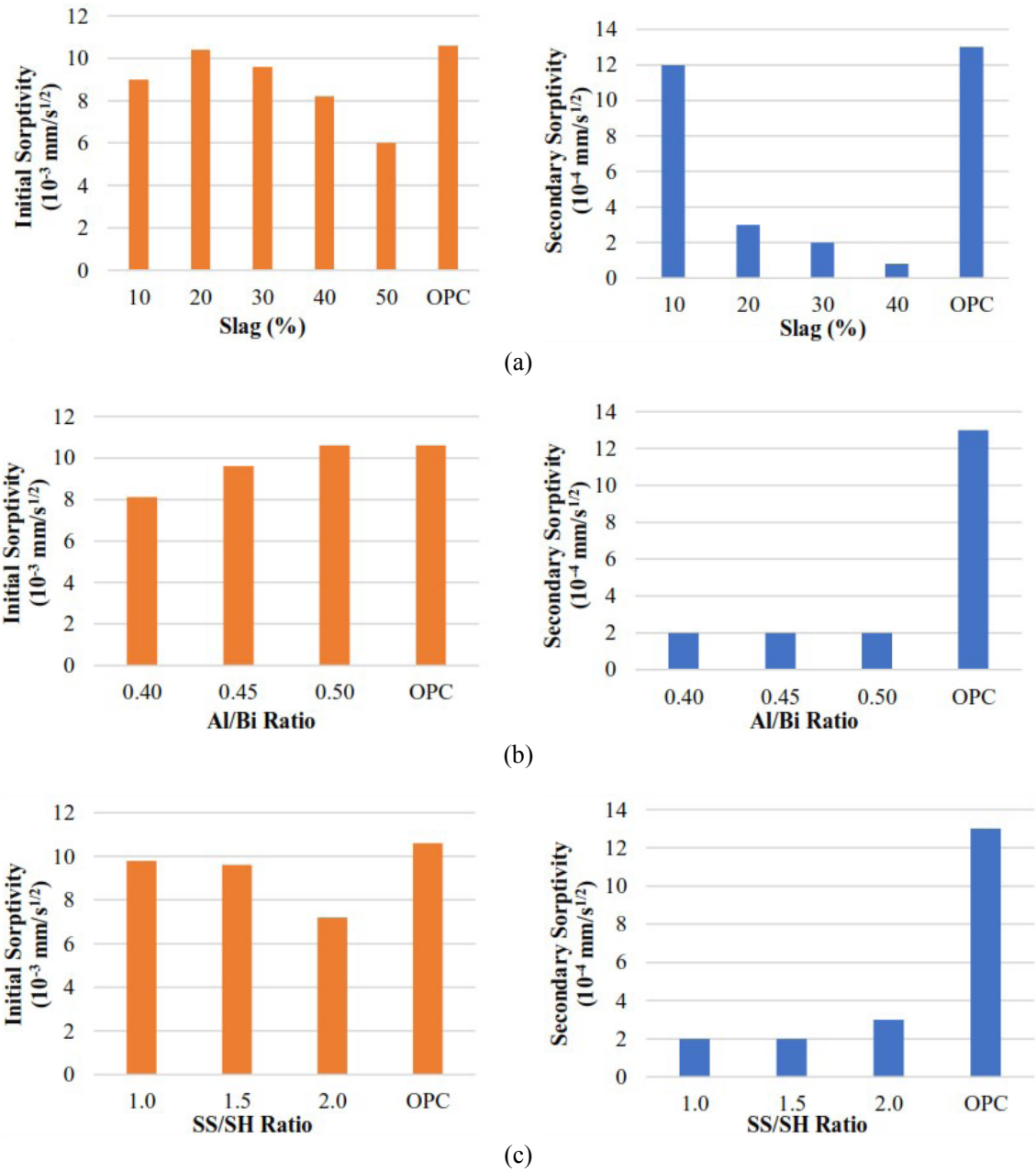

Figure 7. Initial and secondary sorptivity of concrete with (a) variations in the percentage of slag (SS/SH ratio 1.5, Al/Bi ratio 0.45); (b) variations in the Al/Bi ratio (slag 30%, SS/SH ratio 1.5); and (c) variations in the SS/SH ratio (slag 30%, Al/Bi 0.45).

the fact that fly ash/slag concrete has fewer porous capillaries or pores (9). In addition, the less porous matrix is also associated with a smaller slag particle size than the fly ash particles which develops a micro filler effect (22).

As shown in Figure 7(b), the sorptivity coefficient exhibits an increase in conjunction with the rise in the Al/Bi ratio. This can be attributed to the higher volume of liquid present, which results in a more diluted mixture. After the concrete hardens, this dilution leads to the formation of additional capillary pores. The lowest initial sorptivity value of 8.1 x 10^{-3} mm/$s^{1/2}$ was achieved at an Al/Bi ratio of 0.40, followed by Al/Bi ratios of 0.45 and 0.50, which yielded initial sorptivity values of 9.6 x 10^{-3} mm/$s^{1/2}$ and 10.6 x 10^{-3} mm/$s^{1/2}$, respectively. When compared with the initial sorptivity of OPC, GPC has a lower value, but the difference is not significant. This indicates that GPC and OPC have almost the same ability to absorb water at the

beginning of the period. In GPC, variations in the Al/Bi ratio have no effect on secondary sorptivity, whereas the three variations have the same secondary sorptivity. Meanwhile, the value of secondary sorptivity on GPC and OPC differs very significantly. The GPC with all variations of the Al/Bi ratio has a much lower secondary sorptivity of 2 x 10^{-4} mm/$s^{1/2}$, while the OPC is 13 x 10^{-4} mm/$s^{1/2}$. This is because GPC has fewer pores and a denser structure which is indicated by a lower rate of water absorption value than OPC, as seen in Figure 6(b).

Figure 7(c) illustrates the effect of the SS/SH ratio on the sorptivity coefficient. As the SS/SH ratio increases, the initial sorptivity decreases. This decrease was caused by the fact that the alkaline activator was mostly composed of sodium silicate which has a high viscosity. In the end, it leaves fewer pores after the concrete hardens. In addition, the smaller pores at high SS/SH ratios are because the increased silica amount produces denser polymerized gels with superior mechanical characteristics (45). In contrast, the secondary sorptivity shows a direct relationship with the SS/SH ratio. As the SS/SH ratio increases, the secondary sorptivity tends to increase as well, although the observed increase is not substantial. It is worth noting that all GPCs with varying SS/SH ratios exhibited lower initial and secondary sorptivity values compared to OPC. When the SS/SH ratio was 1.0, 1.5, and 2.0, the initial sorptivity value was 9.8, 9.6, and 7.2 x 10^{-3} mm/$s^{1/2}$ and the secondary sorptivity was 2.0, 2.0, and 3.0 x 10^{-4} mm/$s^{1/2}$, respectively. The OPC has an initial and secondary sorptivity value of 10.6 x 10^{-3} mm/$s^{1/2}$ and 13 x 10^{-4} mm/$s^{1/2}$, respectively.

Based on the previous description, it can be seen that the sorptivity coefficient is closely related to the level of water absorption in concrete. The higher the water absorption level, the more the sorptivity coefficient increases. In general, GPC with low molarity SH (2M) and with variations in slag percentage, Al/Bi ratio, and SS/SH ratio has lower sorptivity than OPC. This shows that GPC has a lower rate of water absorption, which is related to the smaller number of pores. So it can be concluded that the sorptivity coefficient is directly proportional to the porosity of the concrete.

3.3. Chloride Permeability

Through the RCPT test, the chloride permeability of GPC was evaluated, as illustrated by the total charge passed value in Figure 8. To further ascertain the depth of chloride penetration, silver nitrate solution ($AgNO_3$) was sprayed on the GPC surface, and the results of this test are displayed in Figure 9.

As seen in Figure 8(a), when the proportion of slag increases as a replacement for fly ash, the chloride permeability of the GPC decreases. This is indicated by the smaller total charged passes. Mixes with slag content of 10%, 20%, 30%, 40%, and 50%, the total charged successively passed was 845.33 C, 739.80 C, 527.18 C, 438.08 C, and 379.13 C, respectively. The presence of calcium-based hydrated materials is responsible for the decreased chloride permeability as the percentage of slag increases, which form together with the geopolymer gel and produce a strong and compact microstructure, thus preventing the entry of chloride ions through pore capillaries. In addition, in the presence of slag, alumina and silica ions (which are very soluble and widely available) will be more easily soluble, thereby increasing the polycondensation mechanism (22). The matrix formed with a decrease in pore size diameter is also associated with a smaller slag particle size than fly ash particles, which develops a micro filler effect (23). The correlation between chloride ion penetration and other pore characteristics, such as tortuosity, is evident according to (18). When fly ash is replaced with slag, the tortuosity of the pore structure increases, which could be a major factor in the decrease of chloride penetration. According to the category in ASTM C 1202-12, all GPC mixtures with varying percentages of slag and OPC have chloride permeabilities in the very low category because they have total charged passes of less than 1000C.

Figure 8(b) shows that the Al/Bi ratio 0.45 produces the least chloride permeability, as indicated by the charged passed value of 527.18 C while the charged passed values of 0.40 and 0.50 Al/Bi ratios were 565.43 C and 628.43 C, respectively. The general trend is that higher Al/Bi ratios will lead to higher porosity and a higher rate of chloride penetration (47). However, as stated in the sub-discussion on porosity, at an Al/Bi ratio of 0.40, the amount of alkaline activator is insufficient for the geopolymerisation process to produce a geopolymeric structure with larger pores (28). Likewise, if the Al/Bi ratio increases from 0.45 to 0.50, the excess alkaline activator that is not used in the geopolymerisation process will leave pores with a larger size and volume. This condition causes higher chloride permeability.

When the SS/SH ratio is increased, the chloride permeability is lessened, as illustrated in Figure 8(c). The highest total charged passed of 560.25 C was noted at SS/SH 1.0, followed by SS/SH 1.5 and SS/SH 2.0, with the total charged passed of 527.18 C and 353.03 C, respectively. At the same SS/SH ratio, the reduction in chloride permeability is in line with the decrease in porosity and sorptivity in concrete. This is because a high SS/SH ratio will increase the silica content and cause the gel to polymerize into a denser matrix, making the pores smaller. In GPC, with all variations of the SS/SH ratio and OPC, it has a very low chloride permeability category because it has a charged passed value of less than 1000 C. When compared to OPC,

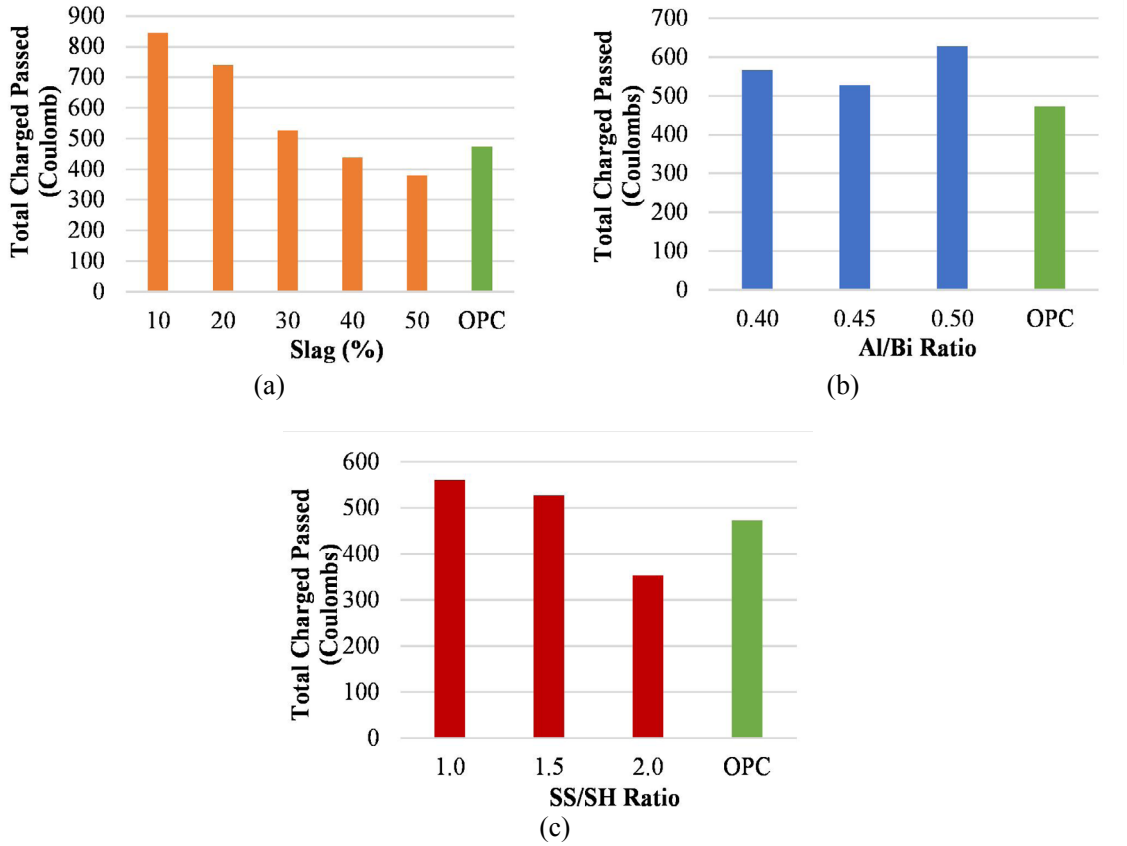

Figure 8. Chloride permeability in GPC concrete with various variations (a) slag percentage (SS/SH ratio 1.5, Al/Bi ratio 0.45); (b) Al/Bi ratio (slag 30%, SS/SH ratio 1.5); and (c) SS/SH ratio (slag 30%, Al/Bi 0.45).

which has a total charged passed of 472.50 C, the mixture of GPC with slag percentages of 40%, 50%, and SS/SH ratio of 2.0 have lower chloride permeability.

Based on Figure 9, the depth of penetration of chloride at various percentages of slag, variations in Al/Bi ratios, and variations in SS/SH ratios is directly proportional to the value of porosity, rate of water absorption, and chloride permeability.

As illustrated in Figure 9(a), an increase in slag content as a replacement for fly ash leads to a decrease in chloride penetration depth. The depth was found to be the greatest (31.5 mm) when 10% slag was used and the lowest (5.7 mm) when 50% slag was used. This phenomenon can be attributed to the dense matrix that slags with a high CaO content creates, resulting in a reduction in the size and number of the concrete pores. Subsequently, the slag in GPC promotes a lower amount of chloride attack since the chlorides penetrate concrete through capillary pores. When compared to OPC, GPC based on fly ash-slag has better durability in a chloride environment, as evidenced by a much lower depth of chloride penetration (OPC has a chloride penetration depth of 39.6 mm).

The Al/Bi ratio that produced the lowest chloride penetration depth is 0.45, with a depth of 16.1 mm. At 0.40 and 0.50 ratios of Al/Bi, the GPC has chloride penetration depths of 24.6 mm and 18.0 mm, respectively, as shown in Figure 9(b). Meanwhile, Figure 9(c) shows that geopolymer concrete with a minimum chloride penetration depth of 16.1 mm is noted at an SS/SH ratio of 1.5. The SS/SH ratios of 1.0 and 2.0 result in deeper penetration depths of 24.3 mm and 18.2 mm, respectively. Compared with OPC, which has a chloride penetration depth of 39.6 mm, GPC exhibits a much lower penetration depth for all variations of the Al/Bi ratio and SS/SH ratio. These levels of chloride penetration depth can be seen in Figure 10.

The depth of chloride ion penetration in concrete relates to the amount and size of pores, water absorption, and the presence of external pressure. Based on the previous description, GPC with SH 2M molarity has fewer and smaller pores, as well as lower water absorption. As a result, GPC has a lower chloride ion penetration depth and greater resistance to chloride attack than OPC.

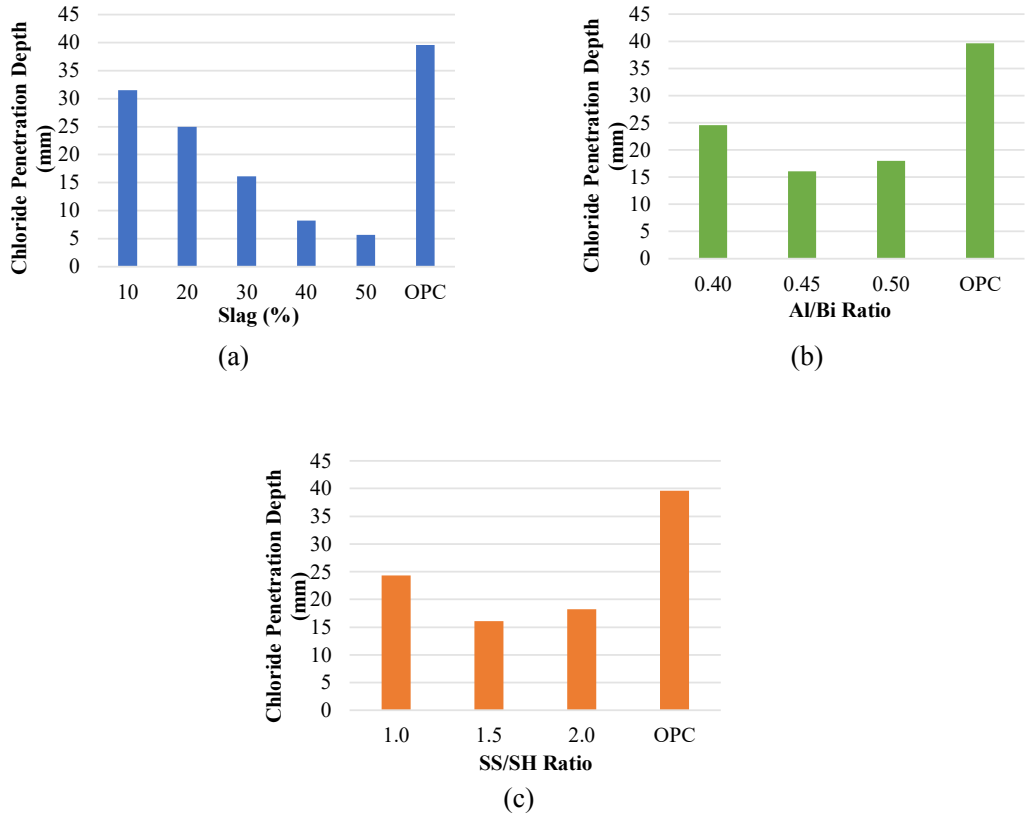

Figure 9. The relationship between the depth of chloride penetration with variations (a) the percentage of slag (SS/SH ratio 1.5, Al/Bi ratio 0.45); (b) the Al/Bi ratio (slag 30%, SS/SH ratio 1.5); and (c) SS/SH ratio (slag 30%, Al/Bi 0.45).

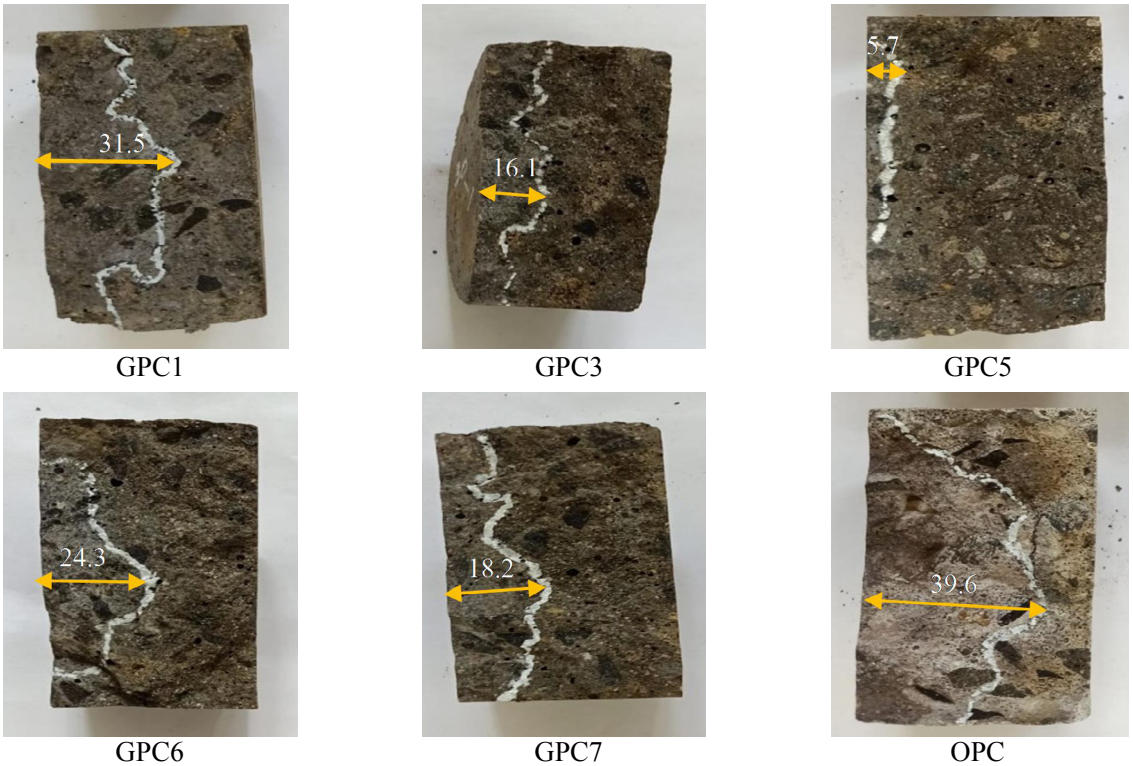

Figure 10. Depth of chloride penetration in GPC1, GPC3, GPC5, GPC6, GPC7 and OPC.

CONCLUSIONS

In this paper, the results of the research are presented for the effect of low molarity SH (2M) with variations in slag percentages, variations in SS/SH ratios, and variations in Al/Bi ratios on porosity, sorptivity and chloride permeability in fly ash-slag-based GPC. Based on the results of the study it can be concluded that:

- The higher the percentage of slag as a substitute for fly ash, and the higher the SS/SH ratio, the lower the porosity of the concrete. A slag content of 50% and SS/SH ratio of 2.0 resulted in the lowest porosities (7.53% and 7.65%, respectively). Meanwhile, the Al/Bi ratio that produces minimum porosity, is the Al/Bi ratio of 0.45 (8.82%). All GPC has lower porosity than OPC.
- Increasing the slag percentage and ratio of SS/SH reduces the level of water absorption and sorptivity. The lowest sorptivity was 6 x 10^{-3} mm/$s^{1/2}$ and 7.2 x 10^{-3} mm/$s^{1/2}$, obtained at 50% slag content and an SS/SH ratio of 2.0. The increase in the Al/Bi ratio causes the sorptivity of concrete to increase. Meanwhile, the lowest water absorption rate was obtained at an Al/Bi ratio of 0.45. All variations of GPC mixes have lower levels of water absorption and sorptivity than OPC.
- The higher the slag percentage and ratio of SS/SH, the lower the chloride permeability. The lowest chloride permeability was obtained at 50% slag content and an SS/SH ratio of 2.0, with a total charged passed of 379.13 C and 352.03 C, respectively. The optimal Al/Bi ratio is 0.45, which produces the lowest total charged passed of 527.18 C.
- When compared to OPC, the mixture of GPC with slag percentage of 40%, 50%, and SS/SH ratio of 2.0 have lower chloride permeability. All mixtures, both GPC and OPC have chloride permeabilities in the very low category because they have total charged passes of less than 1000C.
- The lowest chloride penetration depth was obtained at a 50% slag content (GPC5) of 5.7 mm and the highest at a 10% slag content (GPC1) of 31.5 mm. All chloride penetration depths in GPC are lower than OPC, with a chloride penetration depth of 39.6 mm.
- The recommended proportions of fly ash-slag based GPC mixes with porosity, sorptivity, and chloride permeability lower than OPC are GPC4 (slag 40%, SS/SH ratio 1.5, Al/Bi ratio 0.45); GPC5 (slag 50%, SS/SH ratio 1.5, Al/Bi ratio 0.45); and GPC7 (slag 30%, SS/SH ratio 2.0, Al/Bi ratio 0.45).

Data availability

The data presented in this study are available on request from the corresponding author.

Acknowledgments

The authors are sincerely grateful to Kementerian Pendidikan, Kebudayaan, Riset dan Teknologi, Indonesia for funding research support; Universitas Sebelas Maret Surakarta, Indonesia for supporting laboratories and research equipment; Tanjung Jati B Power Plant, Jepara, Indonesia; PT. Krakatau Semen Indonesia, Cilegon, Indonesia; and PT. Panca Beton, Karanganyar, Indonesia to support research materials.

Funding sources

The research and publication of this paper have been made possible due to financial support from Direktorat Riset, Teknologi dan Pengabdian kepada Masyarakat, Direktorat Jenderal Pendidikan Tinggi, Riset dan Teknologi with Universitas Sebelas Maret, Contract Number: 673.1/UN27.22/PT.01.03/2022 and No. 096/E5/PG.02.00.PT/2022.

Authorship contribution statement

Ernawati Sri Sunarsih: Conceptualization, Formal analysis, Methodology, Funding acquisition, Writing – original draft, Writing – review & editing.

Sholihin As'ad: Conceptualization, Methodology, Supervision, Validation.

Abdul Rahman Mohd Sam: Supervision, Validation, Writing – review & editing.

Stefanus A. Kristiawan: Conceptualization, Methodology, Supervision, Validation, Writing – review & editing, Fund raising.

Declaration of competing interest

The authors of this article declare that they have no financial, professional or personal conflicts of in-terest that could have inappropriately influenced this work.

REFERENCES

1. Davidovits J. 2013. Geopolymer cement a review. Geopolymer Institute. 1–11. Retrieved from https://www.geopolymer.org/library/technical-papers/21-geopolymer-cement-review-2013/.
2. Turner LK, Collins FG. 2013. Carbon dioxide equivalent (CO_2-e) emissions: A comparison between geopolymer and OPC cement concrete. Constr. Build. Mater. 43:125–130. http://doi.org/10.1016/j.conbuildmat.2013.01.023.
3. Yang K, Song J, Song K. 2013. Assessment of CO_2 reduction of alkali-activated concrete. J. Clean. Prod. 39:265–72. http://doi.org/10.1016/j.jclepro.2012.08.001
4. Olivier JGJ, Peters JAHW. 2019. Trends in global CO_2 and total greenhouse gas. Summary of the 2019 Report. PBL Netherlands Environmental Assessment Agency PBL publication number: 4004. Netherlands.
5. Tennakoon C, Shayan A, Sanjayan JG, Xu A. 2017. Chloride ingress and steel corrosion in geopolymer concrete based

on long term tests. Mater. Des. 116:287–299. http://doi.org/10.1016/j.matdes.2016.12.030.
6. Neupane K. 2016. Fly ash and GGBFS based powder-activated geopolymer binders: A viable sustainable alternative of portland cement in concrete industry. Mech. Mater. 103:110–122. http://doi.org/10.1016/j.mechmat.2016.09.012.
7. Zannerni GM, Fattah KP, Al-Tamimi AK. 2020. Ambient-cured geopolymer concrete with single alkali activator. Sustain. Mater. Techno. 23:e00131. https://doi.org/10.1016/j.susmat.2019.e00131.
8. Okoye FN, Durgaprasad J, Singh NB. 2016. Effect of silica fume on the mechanical properties of fly ash based-geopolymer concrete. Ceram. Int. 42(2, Part B):3000–6. http://doi.org/10.1016/j.ceramint.2015.10.084.
9. Angulo-Ramírez DE, Valencia-Saavedra WG, Mejía de Gutiérrez R. 2020. Alkali-activated concretes based on fly ash and blast furnace slag: Compressive strength water absorption and chloride permeability. Ing. Investig. 40(2):72–80. https://doi.org/10.15446/ing.investig.v40n2.83893.
10. Mehta A, Siddique R. 2016. An overview of geopolymers derived from industrial by-products. Constr. Build. Mater. 127:183–98. http://doi.org/10.1016/j.conbuildmat.2016.09.136.
11. Part WK, Ramli M, Cheah CB. 2015. An overview on the influence of various factors on the properties of geopolymer concrete derived from industrial by-products. Constr. Build. Mater. 77:370–395. http://doi.org/10.1016/j.conbuildmat.2014.12.065.
12. Singh B, Ishwarya G, Gupta M, Bhattacharyya SK. 2015. Geopolymer concrete: A review of some recent developments. Constr. Build. Mater. 85:78–90. http://doi.org/10.1016/j.conbuildmat.2015.03.036.
13. Noushini A, Castel A. 2016. The effect of heat-curing on transport properties of low-calcium fly ash-based geopolymer concrete. Constr. Build. Mater. 112:464–477. http://doi.org/10.1016/j.conbuildmat.2016.02.210.
14. Alanazi H, Hu J, Kim YR. 2019. Effect of slag silica fume and metakaolin on properties and performance of alkali-activated fly ash cured at ambient temperature. Constr. Build. Mater. 197:747–756. https://doi.org/10.1016/j.conbuildmat.2018.11.172.
15. Cheng Y, Hongqiang M, Hongguang Z, Weijian L, Minglang X, Yilei Liu YG. 2018. Study on chloride binding capability of coal gangue based cementitious materials. Constr. Build. Mater. 167:649–656. https://doi.org/10.1016/j.conbuildmat.2018.02.071.
16. Rafeet A, Vinai R, Soutsos M, Sha W. 2019. Effects of slag substitution on physical and mechanical properties of fly ash-based alkali activated binders (AABs). Cem. Concr. Res. 122:118–35. https://doi.org/10.1016/j.cemconres.2019.05.003.
17. Yousefi Oderji S, Chen B, Ahmad M.R, Shah SFA. 2019. Fresh and hardened properties of one-part fly ash-based geopolymer binders cured at room temperature: Effect of slag and alkali activators. J. Clean. Prod. 225:1–10. https://doi.org/10.1016/j.jclepro.2019.03.290.
18. Provis JL, Myers RJ, White CE, Rose V, Van Deventer JSJ. 2012. X-ray microtomography shows pore structure and tortuosity in alkali-activated binders. Cem. Concr. Res. 42(6):855–64. http://doi.org/10.1016/j.cemconres.2012.03.004.
19. Lee NK, Lee HK. 2016. Influence of the slag content on the chloride and sulfuric acid resistances of alkali-activated fly ash/slag paste. Cem. Concr. Compos. 72:168–79. http://doi.org/10.1016/j.cemconcomp.2016.06.004.
20. Deb PS, Nath P, Sarker PK. 2015. Drying shrinkage of slag blended fly ash geopolymer concrete cured at room temperature. Procedia. Eng. 125:594–600. http://doi.org/10.1016/j.proeng.2015.11.066.
21. Hu Y, Tang Z, Li W, Li Y, Tam VWY. 2019. Physical-mechanical properties of fly ash/GGBFS geopolymer composites with recycled aggregates. Constr. Build. Mater. 226:139–151. https://doi.org/10.1016/j.conbuildmat.2019.07.211.
22. Mehta A, Siddique R, Özbakkaloglu T, Shaikh FUA, Belarbi R. 2020. Fly ash and ground granulated blast furnace slag-based alkali-activated concrete: Mechanical transport and microstructural properties. Constr. Build. Mater. 257:1–10. https://doi.org/10.1016/j.conbuildmat.2020.119548.
23. Khan MZN, Shaikh F uddin A, Hao Y, Hao H. 2016. Synthesis of high strength ambient cured geopolymer composite by using low calcium fly ash. Constr. Build. Mater. 125:809–820. http://doi.org/10.1016/j.conbuildmat.2016.08.097.
24. Arbi K, Nedeljković M, Zuo Y, Ye G. 2016. A review on the durability of alkali-activated fly ash/slag systems: advances issues and perspectives. Ind. Eng. Chem. Re. 55(19):5439–5453. https://pubs.acs.org/doi/abs/10.1021/acs.iecr.6b00559.
25. Ismail I, Bernal SA, Provis JL, Nicolas RS, Nicolas RS, Brice DG, et al. 2013. Influence of fly ash on the water and chloride permeability of alkali-activated slag mortars and concretes. Constr. Build. Mater. 48:1187–1201. https://doi.org/10.1016/j.conbuildmat.2013.07.106.
26. Babaee M, Castel A. 2018. Chloride diffusivity chloride threshold and corrosion initiation in reinforced alkali-activated mortars: Role of calcium alkali and silicate content. Cem. Concr. Res. 111:56–71. https://doi.org/10.1016/j.cemconres.2018.06.009.
27. Noushini A, Castel A, Aldred J, Rawal A. 2020. Chloride diffusion resistance and chloride binding capacity of fly ash-based geopolymer concrete. Cem. Concr. Compos. 105:103290. https://doi.org/10.1016/j.cemconcomp.2019.04.006.
28. Bellum RR, Muniraj K, Madduru SRC. 2020. Influence of slag on mechanical and durability properties of fly ash-based geopolymer concrete. J. Korean Ceram. Soc. 57(5):530–45. https://doi.org/10.1007/s43207-020-00056-7.
29. Değirmenci FN. 2018. Utilization of natural and waste pozzolans as an alternative resource of geopolymer mortar. Int. J. Civ. Eng. 16(2):179–88. https://doi.org/10.1007/s40999-016-0115-1.
30. Lee WH, Wang JH, Ding YC, Cheng TW. 2019. A study on the characteristics and microstructures of GGBS/FA based geopolymer paste and concrete. Constr. Build. Mater. 211:807–13. https://doi.org/10.1016/j.conbuildmat.2019.03.291.
31. Reddy DV, Edouard JB, Sobhan K. 2013. Durability of fly ash–based geopolymer structural concrete in the marine environment. J. Mater. Civ. Eng. 25(6):781–7. https://doi.org/10.1061/(asce)mt.1943-5533.0000632.
32. Kayali O, Khan MSH, Sharfuddin Ahmed M. 2012. The role of hydrotalcite in chloride binding and corrosion protection in concretes with ground granulated blast furnace slag. Cem. Concr. Compos. 34(8):936–45. http://doi.org/10.1016/j.cemconcomp.2012.04.009.
33. Mallikarjuna Rao G, Gunneswara Rao TD. 2018. A quantitative method of approach in designing the mix proportions of fly ash and GGBS-based geopolymer concrete. Aust. J. Civ. Eng. 16(1):53–63. https://doi.org/10.1080/14488353.2018.1450716.
34. Nagajothi S, Elavenil S. 2021. Effect of GGBS addition on reactivity and microstructure properties of ambient cured fly ash based geopolymer concrete. Silicon. 13(2):507–516. https://doi.org/10.1007/s12633-020-00470-w.
35. El-Hassan H, Ismail N. 2018. Effect of process parameters on the performance of fly ash/GGBS blended geopolymer composites. J. Sustain. Cem. Mater. 7(2):122–40. https://doi.org/10.1080/21650373.2017.1411296.
36. Habert G, D'Espinose de Lacaillerie JB, Roussel N. 2011. An environmental evaluation of geopolymer based concrete production: Reviewing current research trends. J. Clean. Prod. 19(11):1229–38. http://doi.org/10.1016/j.jclepro.2011.03.012.
37. Yang KH, Song JK, Song KIl. 2013. Assessment of CO_2 reduction of alkali-activated concrete. J. Clean. Prod. 39:265–72. http://doi.org/10.1016/j.jclepro.2012.08.001.
38. Mclellan BC, Williams RP, Lay J, Riessen AV, Corder GD. 2011. Costs and carbon emissions for geopolymer pastes in comparison to ordinary portland cement. J. Clean. Prod. 19(9–10):1080–1090. http://doi.org/10.1016/j.jclepro.2011.02.010.
39. Badan Standarisasi Nasional. 2012. SNI 7656:2012: Tata cara pemilihan campuran untuk beton normal beton berat dan beton massa. badan standarisasi nasional jakarta indones.
40. Committee 211 ACI. 2009. ACI 211.1-91: Standard practice for selecting proportions for normal heavyweight and mass concrete. ACI Stand.
41. ASTM International. 1997. ASTM C642-97: Standard test method for density absorption and voids in hardened concrete. ASTM Int United States.
42. ASTM International. 2018. ASTM C1585-13: Standard test method for measurement of rate of absorption of water by hydraulic cement concretes. In: ASTM International.

43. ASTM International. 2012. ASTM C1202-12: Standard test method for electrical indication of concrete's ability to resist chloride ion penetration. American Society for Testing and Materials.
44. Aiken TA, Kwasny J, Sha W, Soutsos MN. 2018. Effect of slag content and activator dosage on the resistance of fly ash geopolymer binders to sulfuric acid attack. Cem. Concr. Res. 111:23–40. https://doi.org/10.1016/j.cemconres.2018.06.011.
45. Puertas F, Palacios M, Manzano H, Dolado JS, Rico A, Rodríguez J. 2011. A model for the C-A-S-H gel formed in alkali-activated slag cements. J. Eur. Ceram. Soc. 31(12):2043–2056. http://doi.org/10.1016/j.jeurceramsoc.2011.04.036.
46. Kristiawan SA, Sunarmasto, Ridlo MM. 2018. Sorptivity of self-compacting concrete with high volume fly ash and its eco-mechanical-durability performance. IOP Conf. Ser. Mater. Sci. Eng. 442(1):012002. https://doi.org/10.1088/1757-899X/442/1/012002.
47. Zhu H, Zhang Z, Zhu Y, Tian L. 2014. Durability of alkali-activated fly ash concrete: Chloride penetration in pastes and mortars. Constr. Build. Mater. 65:51–9. http://doi.org/10.1016/j.conbuildmat.2014.04.110.